

Stability of a microvessel subject to structural adaptation of diameter and wall thickness

ILARI SHAFER, RACHEL NANCOLLAS, MORGAN BOES AND ALISHA L. SIEMINSKI
Franklin W. Olin College of Engineering, Needham, MA 02492, USA

AND

JOHN B. GEDDES*

*Franklin W. Olin College of Engineering, Needham, MA 02492 USA and
Institute for Complex Systems and Mathematical Biology, University of Aberdeen,
AB42 3FX Aberdeen, UK*

*Corresponding author: john.geddes@olin.edu

[Received on 4 May 2009; revised on 12 February 2010; accepted on 20 July 2010]

Vascular adaptation—or structural changes of microvessels in response to physical and metabolic stresses—can influence physiological processes like angiogenesis and hypertension. To better understand the influence of these stresses on adaptation, Pries *et al.* (1998, 2001a,b, 2005) have developed a computational model for microvascular adaptation. Here, we reformulate this model in a way that is conducive to a dynamical systems analysis. Using these analytic methods, we determine the equilibrium geometries of a single vessel under different conditions and classify its type of stability. We demonstrate that our closed-form solution for vessel geometry exhibits the same regions of stability as the numerical predictions of Pries *et al.* (2005, Remodeling of blood vessels: responses of diameter and wall thickness to hemodynamic and metabolic stimuli. *Hypertension*, **46**, 725–731). Our analytic approach allows us to predict the existence of limit-cycle oscillations and to extend the model to consider a fixed pressure across the vessel in addition to a fixed flow. Under these fixed pressure conditions, we show that the vessel stability is affected and that the multiple equilibria can exist.

Keywords: microvascular; adaptation; stability.

1. Introduction

The primary function of the cardiovascular system is to transport oxygen and nutrients to and provide waste removal from tissues. While this exchange occurs in the capillaries, regulation of the cardiovascular system occurs systemically. Homeostasis is maintained through a complex feedback system, which includes modulation of the pumping capability of the heart and the resistance of the microvasculature. In particular, structural remodelling of the body's small blood vessels occurs continuously in response to changing hemodynamic conditions—namely flow rate and pressure—so as to maintain appropriate blood flow to the organs and tissues. Vascular remodelling is an important part of the response to changing conditions that occur in physiological events such as development, endurance training and pregnancy (Buus *et al.*, 2001). However, vascular remodelling, normal or impaired, may also play a role in the pathologies associated with conditions such as hypertension, diabetes and collateral formation after ischemic injury (Dumont *et al.*, 2007).

During remodelling, vessels may change in size and may also be added, as seen in angiogenesis, or die off, as seen in capillary network pruning (Dor *et al.*, 2001), without compromising the stability of adjacent vessels (Araujo & McElwain, 2004). An understanding of this structural remodelling of the microvasculature has great relevance to numerous physiological and pathological events. However, the small size of microvessels, on the order of $10^3 \mu\text{m}$ long and $25\text{--}45 \mu\text{m}$ in diameter (Pozrikidis, 2003) and the challenges of reproducing their behaviour over time *in vivo* or *in vitro*, makes experimental work quite difficult (Chrobak *et al.*, 2006). In order to obtain a more complete and broadly applicable understanding of how microvessels change over time, mathematical models can be useful in predicting how vessels will react to changes in their environment without subjecting actual vessels to those stresses (Perktold & Rappitsch, 1995).

Though we focus on analysis of a specific model, it should be noted that vascular remodelling and angiogenesis are rather active topics in mathematical biology. They are discussed in a recent review of the key approaches to modelling microvascular adaptation with regards to angiogenesis (Chaplain *et al.*, 2006). These models have explored vascular adaptation in healthy tissue (Owen *et al.*, 2009) and in the capillary networks surrounding tumours, which have been of demonstrated importance in tumour development (Stephanou *et al.*, 2006). Some of these models suggest that the adaptation of microvessels surrounding tumours are critical factors in the angiogenesis that feeds tumour growth (Mcdougall *et al.*, 2002; Bartha & Rieger, 2006).

Here, we consider a model for microvascular structural adaptation developed over the past decade by Pries *et al.* (1998, 2001a,b, 2005). Their computational model describes the diameter and width of a vessel with two coupled differential equations. By conducting a set of careful numerical experiments, the authors found a set of model parameters that lead to stable vessels with geometries that are well matched to *in vivo* findings. These vessels adapt towards an equilibrium diameter and width instead of collapsing, oscillating or expanding to unreasonable dimensions. We use the tools of dynamical systems to analyse the model in detail and find that our results from reformulating the model match the numerical conclusions of Pries *et al.* (1998, 2001a,b, 2005).

Our first exploration considers a single vessel with a fixed blood flow. We formulate the equations of the model of Pries *et al.* (1998, 2001a,b, 2005) in a coherent system and describe the physical and metabolic stimuli that cause vascular remodelling. These stimuli are combined into a pair of differential equations that describe remodelling. Using analytic techniques, we obtain a closed-form solution for the single equilibrium solution under the fixed flow condition. We analyse the type of stability at this equilibrium and find that the region of stability predicted by our dynamical systems approach matches the region found in the numerical simulation of Pries *et al.* (1998, 2001a,b, 2005). We also find evidence of limit-cycle oscillations in which the vessel diameter and width continuously go through a process of expansion and contraction. Expanding the analysis, we consider the model when the pressure drop across the vessel is fixed instead of the flow. We find that two equilibria are present in this case, although only one is stable. In this way, we explore the proposed model for a single vessel using tools from dynamical systems.

2. Adaptation model

The model of structural adaptation we consider is a mathematical model proposed by Pries *et al.* (2005). Here, we focus our attention on a single vessel and synthesize the model from several of the group's published works to develop a straightforward set of differential equations and a closed-form representation of vessel diameter (Pries *et al.*, 1998, 2001a,b, 2005). The vessel we consider has the geometry shown in Fig. 1 and is modelled as a tube of fixed length and uniform wall thickness with Poiseuille

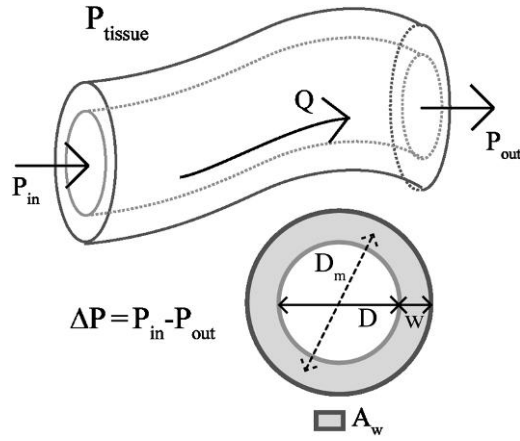


FIG. 1. Schematic of single vessel. The pressure drop across the vessel of length L is ΔP and the flow through the vessel is Q . The vessel has lumen D , wall width w , mid-wall diameter $D_m = D + w$ and cross-sectional wall area $A_w = \pi w D_m$.

flow. The boundary conditions of this model are flexible and can be posed in terms of either a fixed flow Q or fixed pressure drop ΔP . We first consider a vessel with a fixed flow condition, and then move onto the previously unexplored, but biologically relevant, case of a vessel with a fixed pressure drop. In both cases, we hold the outlet pressure fixed.

The model of Pries *et al.* (1998, 2001a,b, 2005) for microvascular adaptation describes how the mid-wall diameter D_m and cross-sectional area A_w of a vessel adapt over time (Pries *et al.*, 2005). Their model consists of a system of coupled differential equations for each vessel in a network,

$$\frac{dD_m}{dt} = f(D_m, A_w) D_m, \quad (2.1)$$

$$\frac{dA_w}{dt} = g(D_m, A_w) A_w. \quad (2.2)$$

The mid-wall diameter remodelling rate f and cross-sectional area remodelling rate g are each non-linear functions of D_m and A_w and depend on both hemodynamic and metabolic stimuli.

Vascular remodelling is driven by physical stresses on the vessel and chemical stimuli caused by metabolic demand. The two primary physical stresses are shear stress (τ , dependent upon flow through the vessel) and circumferential stress (σ , dependent on the pressure difference, P_T , between the inside and outside of the vessel) (Lehoux & Tedgui, 1998). These physical stresses are combined to form physical stimuli which are functions of the vessel's width, diameter, pressure, flow and other hemodynamic parameters. In addition to these physical stimuli, the model also includes a metabolic stimulus and a conducted stimulus, which depend on blood oxygen levels and represent the surrounding tissue's demand for oxygen.

2.1 Stresses

The wall shear stress τ describes the stress placed on the inner surface of a vessel due to the fluid moving along the sides of the vessel. The shear stress,

$$\tau = \frac{D \Delta P}{4L}, \quad (2.3)$$

can be expressed as a function of the pressure drop ΔP , the vessel length L and the vessel lumen D . Depending on the boundary conditions that are investigated, Q can be substituted into (2.3) by using the relationship between pressure drop and flow

$$\Delta P = \frac{128\eta L Q}{\pi D^4}. \quad (2.4)$$

Circumferential stress is the stress within the vessel walls due to the transmural pressure P_T . Transmural pressure is the pressure difference between the outside of a vessel (P_{tissue} , as shown in Fig. 1) and the average interior pressure. Thus, the circumferential stress,

$$\sigma = \frac{P_T D}{2w}, \quad (2.5)$$

is a function of the transmural pressure P_T , the lumen D and the width w .

2.2 Metabolic stimulus

In addition to physical stresses on the blood vessel, the model includes a chemical stimulus dependent on blood flow. Since tissues require oxygen and other metabolites, chemical signals are released into the bloodstream to increase blood flow when these levels are low. Thus, the metabolic stimulus captures the tissues' demand for additional oxygen. Though a great deal of emphasis is typically placed upon the physical stresses, the biological importance of this stimuli is mirrored by the observation that, mathematically, the metabolic stimulus serves to stabilize vessel networks that would otherwise collapse with only the influence of shear and circumferential stress (Pries *et al.*, 2001a).

The level of available oxygen is described by the saturation of oxygen in the blood $S(\text{PO}_2)$. Oxygen saturation is assumed to decrease linearly down the length L of the vessel due to consumption by the surrounding tissue,

$$S(\text{PO}_2)|_{x=L} = S(\text{PO}_2)|_{x=0} - \frac{k_e L}{2QC_0H}, \quad (2.6)$$

where k_e is the rate at which vessels consume oxygen per unit length, C_0 is the binding constant between oxygen and hemoglobin and H is the hematocrit of blood (Pries *et al.*, 2005). The saturation of oxygen is then converted into partial pressure of oxygen using Hill's equation (Pries *et al.*, 2001a),

$$\text{PO}_2 = P_{50} \left(\frac{S(\text{PO}_2)}{1 - S(\text{PO}_2)} \right)^{1/3}, \quad (2.7)$$

where P_{50} is a reference pressure. This partial pressure is then used to define the level of metabolic signal J_m^{down} at the downstream end of the vessel,

$$J_m^{\text{down}} = J_m^{\text{up}} + \begin{cases} k_m L \left(1 - \frac{\text{PO}_2|_{x=L}}{\text{PO}_{2\text{ref}}} \right) & \text{PO}_2 \leq \text{PO}_{2\text{ref}}, \\ 0 & \text{PO}_2 \geq \text{PO}_{2\text{ref}}, \end{cases} \quad (2.8)$$

where J_m^{up} is the metabolic signal entering the vessel and k_m is the maximum metabolic production rate per unit length. Note that this metabolic signal is conditional on whether the partial pressure of oxygen is above a level given by the reference pressure $\text{PO}_{2\text{ref}}$. In other words, vessels with sufficient oxygen will not produce this metabolic signal.

The metabolic stimulus that acts on a vessel is determined by the amount of metabolite flowing past a given wall area and decreases with increased flow rate. In particular, the metabolic stimulus S_m ,

$$S_m = \ln \left(1 + \frac{J_m}{Q + Q_{\text{ref}}} \right), \quad (2.9)$$

depends on the ratio of the average metabolic signal $J_m = 0.5(J_m^{\text{up}} + J_m^{\text{down}})$ to the flow Q . Q_{ref} is a small value that prevents singular behaviour in vessels with very low flow. Overall, increasing the average metabolic signal increases this stimulus.

2.3 Conducted stimulus

In addition to the metabolic stimulus, vessels also transmit a conducted metabolic stimulus or a metabolic signal that travels upstream, likely via ion channels between cells, when metabolite is needed (Pries *et al.*, 2001a). A conducted metabolic signal J_c^{down} enters a vessel and produces an upstream signal J_c^{up} that is based on itself and the vessel's metabolite. The combined signal depends on J_c^{down} , the metabolic stimulus, and is assumed to decay exponentially with vessel length L ,

$$J_c^{\text{up}} = (J_c^{\text{down}} + S_m)e^{-\frac{L}{L_{\text{ref}}}}, \quad (2.10)$$

where L_{ref} is a reference vessel length. The conducted stimulus S_c ,

$$S_c = \frac{J_c}{J_c + J_0}, \quad (2.11)$$

is a function of the average conducted signal in the vessel $J_c = 0.5(J_c^{\text{down}} + J_c^{\text{up}})$ and a reference value J_0 . This relationship creates a conducted stimulus S_c that increases with S_m and saturates at 1.

2.4 Physical stimuli

While the metabolic stimulus S_m , and conducted stimulus S_c , have a direct effect on vessel adaptation, the impacts of the physical stresses τ and σ are more oblique. The model specifies stimuli S_τ and S_σ ,

$$S_\tau = \frac{\ln \left(\frac{\tau}{\tau_{\text{ref}}} \right)}{1 + k_{w\tau} \ln \left(\frac{w}{w_{\text{ref}}} \right)}, \quad (2.12)$$

$$S_\sigma = \frac{\ln \left(\frac{\sigma}{\sigma_{\text{ref}}} \right)}{1 + k_{w\sigma} \ln \left(\frac{w}{w_{\text{ref}}} \right)}, \quad (2.13)$$

that define how shear and circumferential stresses affect vascular adaptation. These stimuli increase monotonically with increasing stress and decrease with increased vessel width. τ_{ref} , σ_{ref} and w_{ref} give threshold levels at which the stimuli start taking effect and $k_{w\tau}$ and $k_{w\sigma}$ govern the stimuli's dependence on width. Both stimuli increase monotonically with their stress component and decrease with width. These functions capture the natural tendency of vessels to normalize their shear and wall stresses in response to changing stimuli. Specifically, these functions capture the biological observation that increased shear stress tends to cause vasodilation or diameter increase, that in turn returns shear stress to a baseline level. On the other hand, increased wall stress tends to cause vasoconstriction which results in a thicker wall and lowered wall stress.

2.5 Ordinary differential equations

Each vessel is assumed to respond to a linear combination of the four primary stimuli defined in (2.9–2.13). For convenience, these four stimuli are condensed into two effective stimuli $S_{\tau m}$ and $S_{\sigma m}$,

$$S_{\tau m} = S_{\tau} + k_{md}(S_m + k_c S_c) - k_{sd}, \quad (2.14)$$

$$S_{\sigma m} = S_{\sigma} + k_{mg}(S_m + k_c S_c) - k_{sg}, \quad (2.15)$$

where k_{md} , k_{mg} and k_c are parameters that govern the relative strength of metabolic stimuli while k_{sd} and k_{sg} are background stimulus levels (Pries *et al.*, 2001a).

The mid-wall diameter and the cross-sectional area remodelling rates may be expressed as a weighted combination of the effective stimuli $S_{\tau m}$ and $S_{\sigma m}$,

$$\frac{dD_m}{dt} = (R_{\tau d} S_{\tau m} + R_{\sigma d} S_{\sigma m}) D_m, \quad (2.16)$$

$$\frac{dA_w}{dt} = R_w (R_{\tau g} S_{\tau m} + R_{\sigma g} S_{\sigma m}) A_w. \quad (2.17)$$

$R_{\tau d}$, $R_{\tau g}$, $R_{\sigma d}$, and $R_{\sigma g}$ define the relative contributions of each stimulus to the remodelling rate and are normalized such that $R_{\tau d}^2 + R_{\sigma d}^2 = 1$ and $R_{\tau g}^2 + R_{\sigma g}^2 = 1$. $R_{\tau d}$ is assumed to vary on $[0, 1]$, while the other coupling parameters are defined on $[-1, 1]$. R_w defines the relative strength of wall mass remodelling compared to lumen remodelling (Pries *et al.*, 2005).

In Fig. 2, we show the 2D parameter space defined by Pries *et al.* (1998, 2001a,b, 2005) and used in our analysis. Physiologically, shear stress is thought to primarily affect diameter, while circumferential stress primarily affects wall mass. Thus, we define direct coupling as the case when diameter adaptation is purely caused by $S_{\tau m}$ and changes in wall mass are due to $S_{\sigma m}$. These are reflected in the coupling values centred near $R_{\tau d} = 1$, $R_{\tau g} = 0$, $R_{\sigma d} = 0$ and $R_{\sigma g} = 1$ (see black marker in Fig. 2). Notably, cross-coupling, where $S_{\tau m}$ affects A_m and $S_{\sigma m}$ changes D_m , is also possible and is represented by

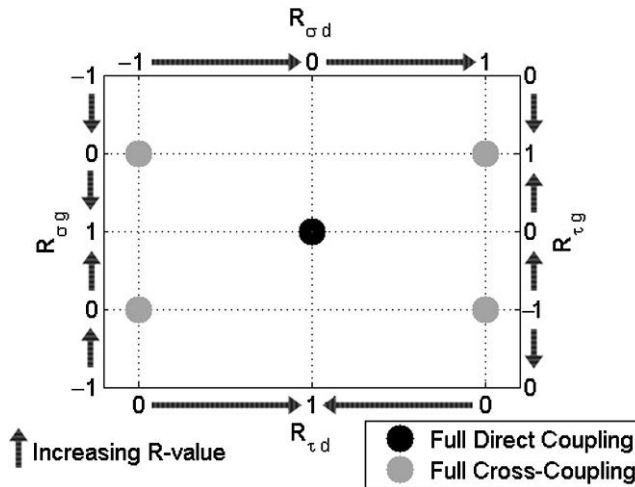


FIG. 2. Two-dimensional coupling space of $R_{\tau d}$, $R_{\tau g}$, $R_{\sigma d}$ and $R_{\sigma g}$ used in our analysis. The R -values represent the relative strength of stimuli. The physiologically sensible direct-coupled set of R -values is located in the centre of the space shown. These R -values vary sinusoidally in the mapping above; arrows denote the direction of increase.

regions where $R_{\tau g}, R_{\sigma d} > 0$. However, large degrees of cross-coupling (see grey markers in Fig. 2) are physiologically abnormal. We will use this parameter space later when we discuss the stability of microvessels under adaptation.

3. Single vessel under constant flow conditions

As previously mentioned, we begin by analyzing a single vessel subject to a fixed flow. We consider a vessel at some initial mid-wall diameter D_m and cross-sectional wall area A_w that adapts over time according to the model presented in (2.3–2.17). The parameter values used in our analysis are typical of a single vessel and are given in Table 1. Without loss of generality, we assume that the metabolic and conducted signals entering the vessel are zero ($J_m^{\text{up}} = 0$ and $J_c^{\text{down}} = 0$). First, we consider the equilibrium solutions and examine their stability.

3.1 Unique equilibrium

In the case when the flow is fixed, one equilibrium is present. To demonstrate this, we solve for the width and diameter where $\frac{dD_m}{dt} = \frac{dA_w}{dt} = 0$. This can occur when either $D_m = 0$ and $A_w = 0$ or when

TABLE 1 Parameter values used in single-vessel analysis for fixed flow as previously specified by Pries *et al.* (1998; 2001a; 2005)

Parameter	Value	Description
τ_{ref}	$0.5598 \frac{\text{dyn}}{\text{cm}^2}$	Reference value for shear stress
σ_{ref}	$32050 \frac{\text{dyn}}{\text{cm}^2}$	Reference value for circumferential stress
w_{ref}	$0.804 \mu\text{m}$	Reference value for width
k_c	1.66	Scale factor for conducted stimulus
k_{md}	0.955	Scale factor for shear metabolic contribution
k_{mg}	-0.374	Scale factor for circumferential metabolic contribution
k_{sd}	3.077	Equilibrium level of $S_{\tau m}$
k_{sg}	0.0177	Equilibrium level of $S_{\sigma m}$
$k_{w\tau}$	0.114	Strength of width influence on $S_{\tau m}$
$k_{w\sigma}$	0.609	Strength of width influence on $S_{\sigma m}$
L	$2000 \mu\text{m}$	Vessel length used in analysis
Q	$9 \frac{\text{nl}}{\text{min}}$	Flow used in analysis
P_{out}	$46655 \frac{\text{dyn}}{\text{cm}^2}$	Pressure at vessel outlet
P_{tissue}	$0 \frac{\text{dyn}}{\text{cm}^2}$	Tissue pressure
C_0	0.5	Percent of oxygen binding to red blood cells
P_{50}	38KPa	Partial pressure of oxygen reference
N	3	Defined in Hill's Equation
k_e	$4 \times 10^{-11} \frac{\text{cm}^3}{\mu\text{m} \cdot \text{min}}$	Derivative of oxygen flux in the vessel
$S(\text{PO}_2) _{x=0}$	0.9398	Initial saturation of oxygen in the vessel
L_{ref}	$14292 \mu\text{m}$	Reference vessel length
J_0	27.9	Basal conducted stimulus
$J_{\text{down}}^{\text{down}}$	0	Downstream conducted signal
J_m^{up}	0	Upstream metabolic signal
$\text{PO}_{2\text{ref}}$	94.4KPa	Reference $P\text{O}_2$ value
Q_{ref}	$10^{-4} \frac{\text{nl}}{\text{min}}$	Reference flow to avoid singularity
H	0.4	Hematocrit

both $S_{\tau m} = 0$ and $S_{\sigma m} = 0$ simultaneously. The first case corresponds to a situation in which vessels collapse, while the second case (in which we are interested) occurs when the net adaptation stimulus is zero. To find this location computationally, we evaluate $S_{\tau m}$ and $S_{\sigma m}$ over a space of D and w . This produces two contours that correspond to $S_{\tau m} = 0$ and $S_{\sigma m} = 0$, respectively. Thus, we are interested in finding the intersection of these contours. Notably, when flow is fixed, S_m and S_c are constant with respect to width and diameter, so they are represented as positive constants, C_1 and C_2 . Therefore, for fixed flow

$$0 = S_{\tau m} = \frac{\ln\left(\frac{\tau}{\tau_{\text{ref}}}\right)}{1 + k_{w\tau} \ln\left(\frac{w}{w_{\text{ref}}}\right)} - C_1 \Rightarrow C_1 + k_{w\tau} C_1 \ln\left(\frac{w}{w_{\text{ref}}}\right) = \ln\left(\frac{\tau}{\tau_{\text{ref}}}\right),$$

$$0 = S_{\sigma m} = \frac{\ln\left(\frac{\sigma}{\sigma_{\text{ref}}}\right)}{1 + k_{w\sigma} \ln\left(\frac{w}{w_{\text{ref}}}\right)} - C_2 \Rightarrow C_2 + k_{w\sigma} C_2 \ln\left(\frac{w}{w_{\text{ref}}}\right) = \ln\left(\frac{\sigma}{\sigma_{\text{ref}}}\right).$$

Since $\ln\left(\frac{w}{w_{\text{ref}}}\right)$, $\ln\left(\frac{\tau}{\tau_{\text{ref}}}\right)$ and $\ln\left(\frac{\sigma}{\sigma_{\text{ref}}}\right)$ are monotonic functions of w , τ and σ , they can only intersect once in the D and w plane. The presence of one intersection corresponds to one equilibrium in the model. Figure (3)a illustrates the presence of a unique equilibrium solution, while Figure (3)b shows that this solution varies with Q such that higher flows lead to narrower vessels.

The existence of a unique equilibrium can also be verified analytically. By solving both $S_{\tau m} = 0$ and $S_{\sigma m} = 0$ for D as a function of w , we obtain closed-form solutions for the curves illustrated in Fig. (3)a. By equating these closed-form functions, we find that there is one value of w , and thus one equilibrium geometry that produces an intersection if flow is fixed,

$$D = \left(\frac{32\eta Q}{\pi \tau_{\text{ref}}} e^{(k_{md}(S_m + k_c S_c) - k_{sd}) \left(1 + k_{w\tau} \ln\left(\frac{w}{w_{\text{ref}}}\right)\right)} \right)^{1/3} \quad (\text{from } S_{\tau m}),$$

$$D = \frac{2w\sigma_{\text{ref}}}{P_T} e^{(k_{mg}(S_m + k_c S_c) - k_{sg}) \left(1 + k_{w\sigma} \ln\left(\frac{w}{w_{\text{ref}}}\right)\right)} \quad (\text{from } S_{\sigma m}).$$

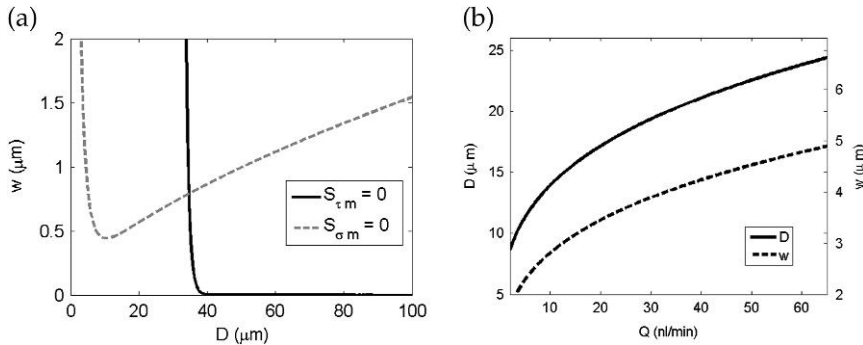


FIG. 3. Existence of a single equilibrium in width and diameter. (a) In the fixed flow case, only one intersection of $S_{\tau m} = 0$ and $S_{\sigma m} = 0$ is present, which corresponds to a single equilibrium. (b) The single equilibrium values of D and w vary with Q .

In addition to confirming the existence of a single equilibrium, we are also interested in the factors that affect the location of the equilibrium. Figure 3(b) illustrates the dependence of equilibrium diameter and width on flow. Although the relationship is not linear due to the presence of metabolic effects, varying Q still produces only one equilibrium. Additionally, the location of the equilibrium is dependent upon the parameters embedded in $S_{\tau m}$ and $S_{\sigma m}$, which represent environmental conditions. Notably, the conditions under which the stimulus terms equal zero are not dependent upon the values of R_w , $R_{\tau d}$, $R_{\tau g}$, $R_{\sigma d}$ and $R_{\sigma g}$.

Having determined the locations of equilibria in the model, we are interested in the behaviour of the equilibrium. Depending on their type of stability, vessels may either approach the equilibrium solution over time or be pushed away from it. Understanding both the equilibrium geometry and its type of stability allows for a better understanding of how vessels adapt in this model.

3.2 Stability of a single equilibrium

Our exploration of stability begins with the numerical results produced in simulation by Pries *et al.* (1998, 2001a,b, 2005). As mentioned above, the equilibrium geometry is not dependent upon $R_{\tau d}$, $R_{\tau g}$, $R_{\sigma d}$, $R_{\sigma g}$ or R_w , but these values do influence the equilibrium's stability.

The aim of our analytic stability investigation is to determine the behaviour of the system around its equilibrium. To do this, we first consider a linear system of ordinary differential equations: $\dot{\mathbf{x}} = \mathbf{A}\mathbf{x}$. Although our system is non-linear, our treatment of the linear case will set the stage for dealing with the non-linear system. It is well accepted that the general solution to a linear system of ordinary differential equations,

$$\mathbf{x}(t) = \sum_j c_j e^{\lambda_j t} \mathbf{v}_j,$$

is a linear combination of the eigenvectors \mathbf{v}_j of the matrix \mathbf{A} . These eigenvectors are weighted with magnitude $c_j e^{\lambda_j t}$ that depends on the eigenvalues λ_j . By inspection of this solution, we conclude that if all the real parts of the eigenvalues are negative, the solution will converge to zero. However, a single eigenvalue with positive real part will lead to divergent behaviour. Thus, to determine the stability of our system, it is necessary to determine the eigenvalues of the relevant linear differential equations. Recall from earlier that our model consists of two coupled, first-order, non-linear differential equations (2.1) and (2.2).

We first linearize the system about the single equilibrium using a Taylor series approximation. This process is discussed in many texts (e.g. Strogatz, 2001). The Jacobian of the system is evaluated at a fixed point. By considering the eigenvalues of the Jacobian, it is found that the system is stable at the fixed point if and only if the trace of the Jacobian is negative and the determinant is positive, and that oscillatory solutions exist if $\text{tr}^2 < 4\Delta$.

Using this analytic method of determining stability, we map the stability regions in Fig. 4(a) onto the R -space shown in Fig. 2. This is done by sweeping the R -values for a given equilibrium and determining the resulting eigenvalues, which allow the equilibrium to be classified. As mentioned above, the type of stability exhibited by an equilibrium depends on these cross-coupling parameters. Mapping these classifications onto the R -space produces Fig. 4(b). White regions represent vessels that converge as a stable spiral, whereas vessels with R -values in the black and dark grey regions do not converge. The centre of the plot, which corresponds to direct coupling, is stable as expected. The stable regions, however, have some degree of cross-coupling, which indicates that D and w are dependent on both $S_{\tau m}$ and $S_{\sigma m}$.

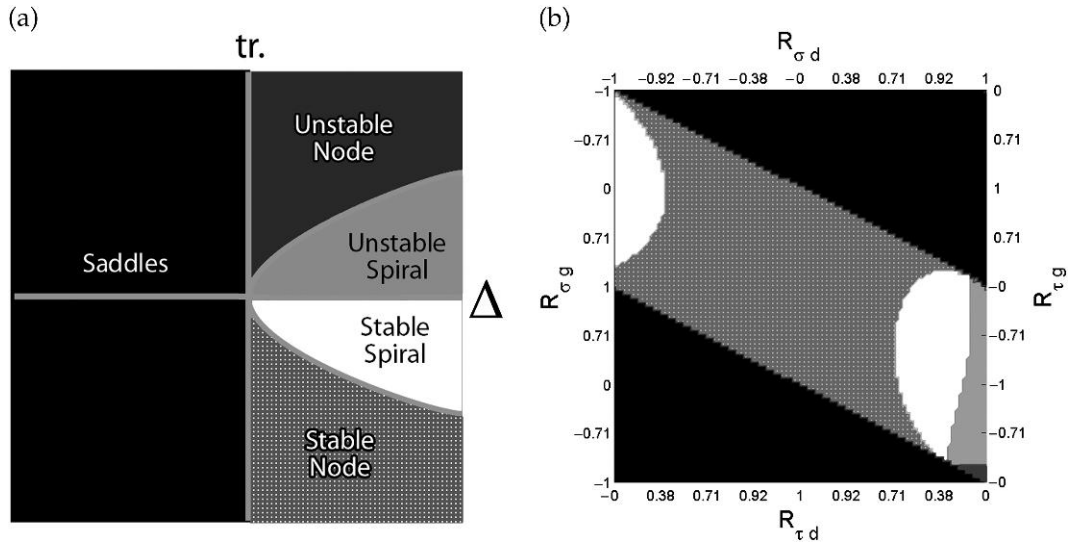


FIG. 4. Analytical regions of stability. The characteristic stability types based on the trace tr and determinant Δ shown in (a) are mapped to the R -space. This region of $R_{\tau d}$, $R_{\tau g}$, $R_{\sigma d}$ and $R_{\sigma g}$ displayed in (b) is the same shown in Fig 2. Examples of the type of behaviour characteristic of the stability regions are provided in Fig. 4(b).

A comparison with the results of Pries *et al.* (1998, 2001a,b, 2005) confirms this analytical stability portrait. The authors performed a stability analysis for the same single-vessel case and also focus on obtaining the dependence of stability on the R -values. Using a simulation for vessel geometry, Pries *et al.* (1998, 2001a,b, 2005) investigate the stability of a single vessel numerically (Pries *et al.*, 1998). After providing the microvessel with initial conditions for D and w , they numerically integrate the system until the magnitudes of $\frac{dD_m}{dt}$ and $\frac{dA_w}{dt}$ are below a threshold value. The time at which the vessel reaches the equilibrium threshold is logged, where low convergence time indicates a stable vessel and failure to converge in a given time limit denotes instability.

Figure 5(a) shows the results obtained by Pries *et al.* (1998, 2001a,b, 2005) over the same space of R -values. It is evident from the numerical results that there is a bounded region in this space where the single vessel will converge to a fixed width and diameter. Notably, this space is akin to the analytical region of stability we find in Fig. 4(b).

Although Pries *et al.* (1998, 2001a,b, 2005) classify stability by convergence time, it is possible to compare these results to our stability analysis. One way of obtaining a metric that is similar to convergence time uses the magnitude of the eigenvalues (Fig. 5(b)). For eigenvalues with a negative real part, a , the magnitude of a determines how quickly the solutions converges along the associated eigenvector. Therefore, when both eigenvalues have a negative real part, the one with the smaller magnitude indicates the upper limit of convergence time. In Fig. 5(b), if the real part of both eigenvalues is negative, we plot the one with the smaller magnitude. Larger values (white) correspond to faster convergence to equilibrium, while smaller values (grey) correspond to slower convergence. The black regions have at least one eigenvalue with a positive real part, so the equilibrium is unstable and does not converge. This classification by magnitude of eigenvalue (based on the analytical stability results) closely matches the computational results from Pries *et al.* (1998, 2001a,b, 2005) shown in Fig. 5(a).

We further validate our stability predictions by simulating the model near the equilibrium. In Fig. 6, we show three examples of the model's trajectory in the (D, w) phase plane corresponding to different

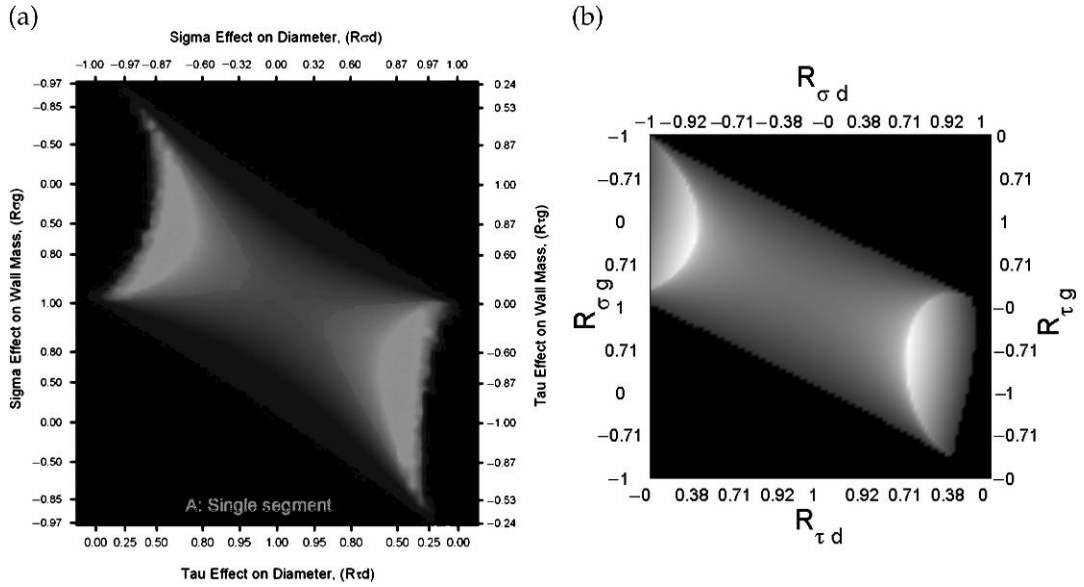


FIG. 5. Comparison to results of Pries *et al.* (a) (used with permission (Pries *et al.*, 2005)). The region of R_{td} , R_{tg} , $R_{\sigma d}$ and $R_{\sigma g}$ is identical to the region in Fig. 4(b). The intensity of the regions in (b) corresponds to $I = \min(|\operatorname{Re}\{\lambda_1\}|, |\operatorname{Re}\{\lambda_2\}|)$, where $\operatorname{Re}\{\lambda_1\}$ and $\operatorname{Re}\{\lambda_2\}$ are negative. White regions correspond to larger I , while grey regions have a smaller I . Black regions denote equilibria with at least one eigenvalue that has a positive real part.

R -values chosen from Fig. 4(b). The presence of stable nodes (a), stable spirals (b) and saddle points (c) is evident. Unstable nodes and spirals are not shown but have phase portraits similar to (a) and (b), respectively. When saddle points, unstable nodes or spirals are present, our modelled vessels either collapse or become unreasonably large. In simulation, we find that these vessels approach a location in the model that is ill defined; approaching zero in D or w produces singularities in the stimulus equations, while moving towards ∞ is highly non-physiological. Further work is needed to conclusively define the behaviour of unstable vessels and the physical meaning of the model in these areas.

We have also found that the limit cycles exist in small regions of the R -space which correspond to unstable spirals. To illustrate this, we choose the point in the R -space shown in Fig. 7(a). The subsequent limit cycle in the (D, w) phase plane is shown in Fig. 7(b). If this limit cycle is viewed as a function of time, we see the oscillations in D and w present in Fig. 7(c). The cause of these oscillations and subsequent limit-cycle behaviour is relatively complex. However, for the fixed flow case, it is important to note that S_m and S_c are not dependent on D or w , so the metabolic and conducted stimuli do not produce oscillations. Instead, the shear and circumferential stresses oscillate, as shown in Fig. 7(d). Although the oscillation of these stresses are both a cause and a result of the oscillation of D and w , the phase shift between τ and σ is not the same as that of D and w . This is due to the cross-coupling in the differential equations, which causes the remodelling of D and w to be dependent on both τ and σ . These oscillations are surprising and raise questions about the limits of the model as well as the long-term behaviour of blood vessels. However, the existence of such oscillations in the human body is questionable because preliminary investigations suggest that the limit cycles tend to occur with unrealistically strong cross-coupling and the behaviour of a single vessel may not be indicative of the behaviour of a network.

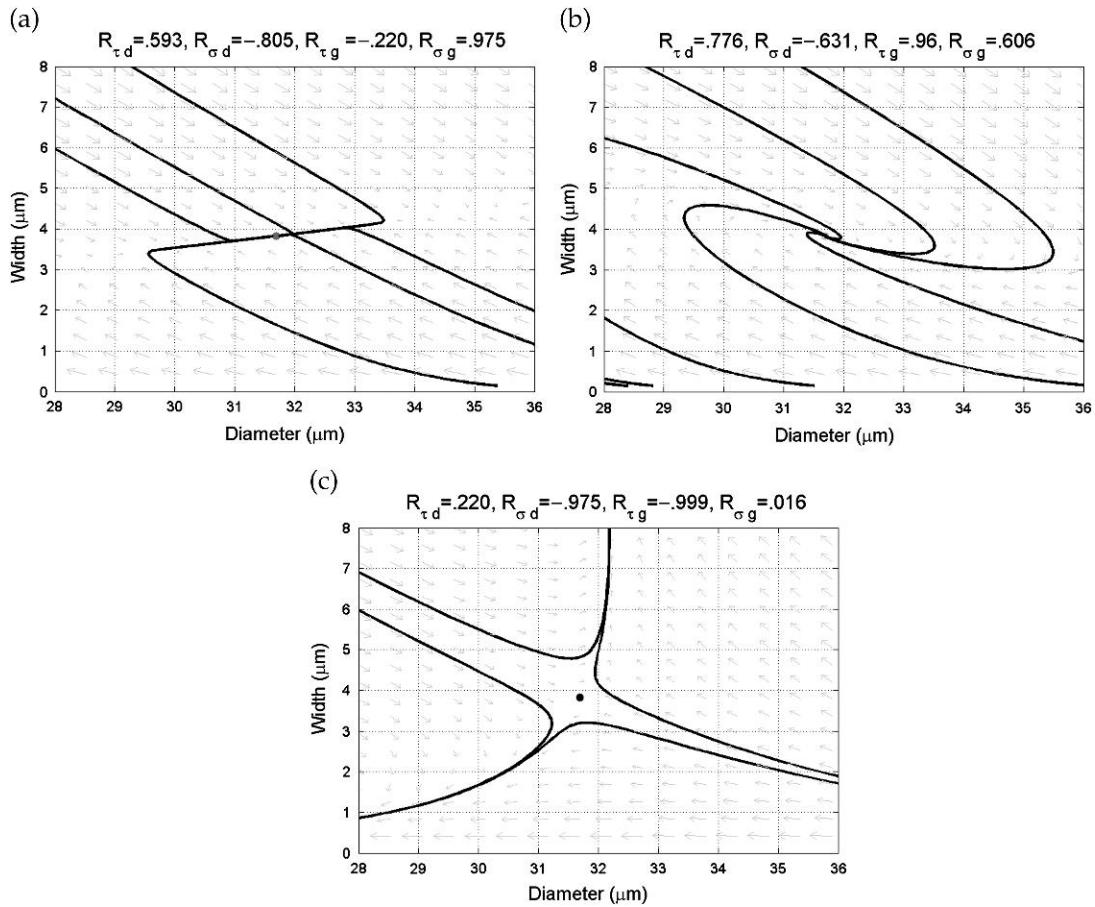


FIG. 6. Examples of dynamic behaviour in the (D, w) phase plane. Dots indicate the type of equilibrium. Each case has different R -values corresponding to Fig. 4(b).

4. Single vessel under constant pressure conditions

Unlike a single vessel, a vascular network has a fixed pressure drop and input flow that feeds vessels in a series–parallel configuration. The result is that actual vessels are regulated by some combination of a fixed flow and fixed pressure case. Therefore, in addition to considering the extreme fixed flow case, we also explore the fixed pressure case for a single vessel. Our analytical work in this area suggests that multiple equilibria are possible, and we examine the stability of these equilibria using the tools developed in the previous section.

4.1 Multiple equilibria

When the pressure ΔP across the vessel is fixed instead of flow, multiple equilibria are possible because the metabolic-derived stimuli S_m and S_c are no longer constant. To determine the locations of multiple equilibria in the (D, w) plane, we perform an analysis similar to the fixed flow case and find locations

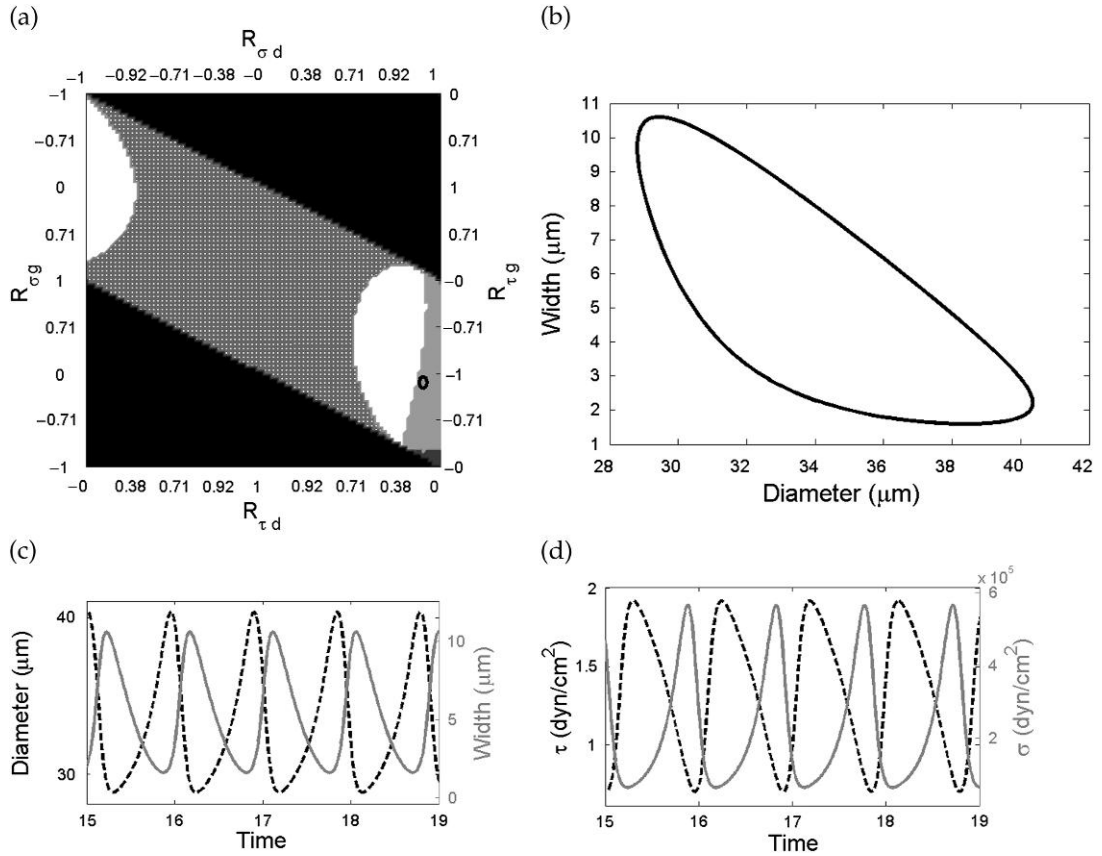


FIG. 7. Unstable spirals can give rise to limit cycles. (a) Location of limit cycle in R -space. (b) Example of limit cycle in (D, w) phase plane. (c) Oscillation of the width and diameter. (d) Oscillation of the stresses, τ and σ . Note that the phase shift between D and w is different from the shift between τ and σ .

where both $S_{\tau m}$ and $S_{\sigma m}$ are equal to zero. The resulting stimulus contours are shown in Fig. 8(a) and the two intersections represent the two equilibria.

The number of equilibria depends on the values of ΔP and P_T . In Fig. 8(b), we show the number of equilibria as a function of P_T and ΔP . For relatively small pressure drops, the vessel can support two equilibrium geometries, while relatively large pressure drops produce no equilibria. The reason for this is that large pressure drops cause high shear stress (τ), which does not support equilibrium geometries.

Although two equilibria are present for many values of ΔP and P_T , physiologically reasonable ΔP for the microvessels under investigation are probably on the order of 10^{-1} mmHg. At these low ΔP , one equilibrium is present at a physiologically reasonable geometry and the other equilibrium is at a much larger D and w . For example, at $\Delta P = 0.1$ mmHg, one equilibrium is present at $D = 34.8 \mu m$ and $w = 8.4 \mu m$, whereas the other is located at $D = 635.0 \mu m$ and $w = 8.4 \mu m$. At higher ΔP , the two equilibria are closer, but such large pressures produce unreasonably large vessel widths. Therefore, the model appears to have only one physiologically reasonable equilibrium even when ΔP and P_T are fixed and multiple equilibria can occur.

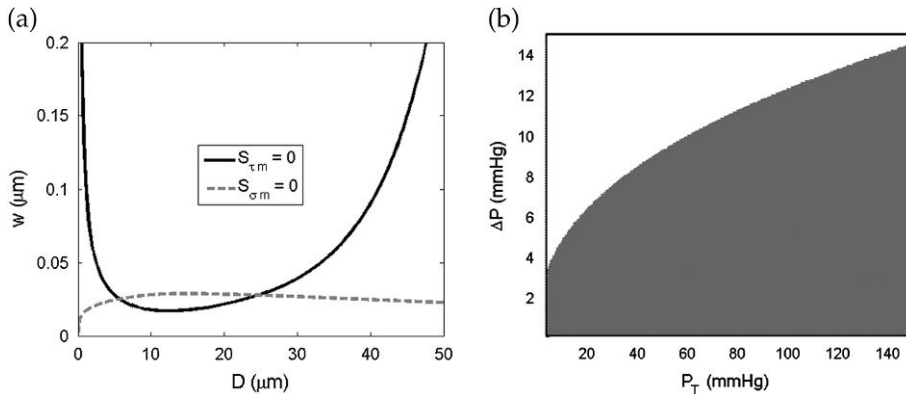


FIG. 8. Existence of multiple equilibria (a) illustrates the existence of two equilibria based on the intersection of contours $S_{\tau m} = 0$ and $S_{\sigma m} = 0$ for $P_T = 10$ mmHg and $\Delta P = 1.5$ mmHg and (b) shows the number of equilibria as a function of P_T and ΔP (white indicates no equilibrium while grey indicates two).

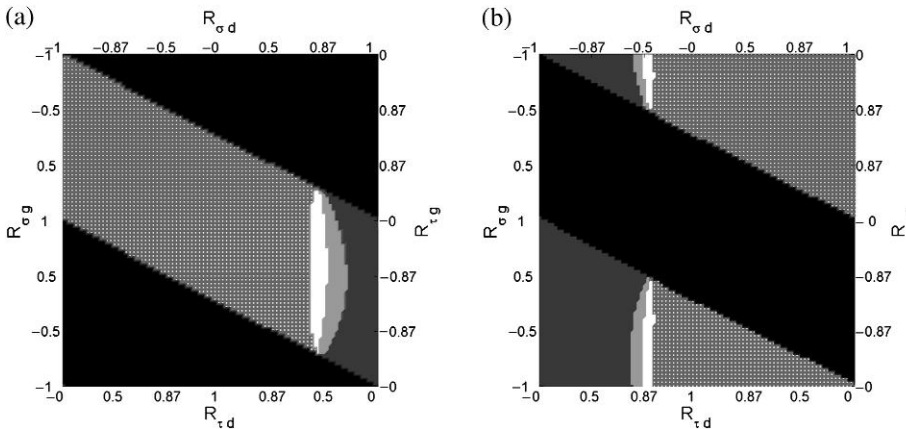


FIG. 9. Regions of stability for equilibrium that are (a) smaller in D and w and (b) larger in D and w . Note that the stability regions are reversed—i.e. the location of saddles for the smaller equilibrium is opposite that of the larger equilibrium. These equilibria are generated when $\Delta P = 10$ mmHg and $P_T = 100$ mmHg.

4.2 Stability of multiple equilibria

When multiple equilibria are present, a natural question concerns whether both equilibria can be stable. That is, for a given set of conditions, are there multiple geometries to which a vessel could converge over time, even if one is physiologically unreasonable? Although we have not obtained analytical confirmation, numerical results suggest that one of the two equilibria will always be a saddle. For example, in Fig. 9, we analyse the stability of the equilibria present when $P_T = 100$ mmHg and $\Delta P = 10$ mmHg. Significantly, the phase portraits of the two equilibria appear to be ‘flipped’, indicating that for a given set of R -values, one of the fixed points is a saddle while the other is a node or spiral. Moreover, under direct coupling ($R_{\tau d} = 1$, $R_{\sigma g} = 1$), the physiologically sensible fixed point is a stable node (as expected) while the unrealistic fixed point is a saddle. This suggests that only one of the system’s equilibria can be stable for a given set of parameters, which means only one vessel geometry is possible in a particular environment.

5. Conclusion

We perform an analysis of the adaptation model proposed by Pries *et al.* (1998, 2001a,b, 2005). In investigating a single vessel with a fixed flow, we compare the regions of stability we found using eigenvalues of our linearized differential equations to the regions of stability determined computationally by Pries *et al.* (1998, 2001a,b, 2005) using convergence time. Our region of stable nodes and stable spirals matches the region of stability previously determined computationally. Likewise, the region of unstable spirals, nodes and saddles corresponds to the coupling parameters Pries *et al.* (1998, 2001a,b, 2005) found were unstable. Moreover, in investigating the boundaries between these regions, we find evidence of limit cycles, which suggests that oscillation of vascular geometry may occur. In an extension of the model, we consider the case when the pressure drop ΔP and transmural pressure P_T are both fixed. In this situation, we find that multiple equilibria are present but that only one of these equilibria is stable for a given set of R -values. Although multiple equilibria are possible, only one equilibrium is physiologically reasonable, so vessels are unlikely to attain two distinct geometries under identical conditions.

A number of unanswered questions about these equilibria and the model remain—for example, the meaning of the equilibrium at $D = 0$ and $w = 0$, where many relationships behave erratically. To address this issue, Pries *et al.* (1998, 2001a,b, 2005) define ‘cut-off’ values for both D and w below which vessels are assumed to collapse. Implementing a continuous extension of this cut-off could provide a better model of vessel collapse and generation. Also, there are certain R -values that can lead to runaway growth of the vessel, which could be adjusted to eliminate this unrealistic feature of the current model. More importantly, the mathematical analysis presented here could be extended to small networks of vessels which could provide more insight into the nature and stability of equilibria in networks.

In general, analytical investigation of the model of Pries *et al.* (1998, 2001a,b, 2005)—and similar biological models—can yield stronger conclusions about the behaviour of the system than computational studies alone. For example, an analytical exploration of stability allows for determination of the type of stability rather than simply a knowledge of convergence times. At a higher level, mathematical analysis indicates the conditions that lead to stable vessels and the boundaries of a model, which are of physiological interest. Often, this data cannot be obtained through direct experimentation, so mathematical analysis can be used as a tool for studying otherwise intractable systems. Finally, from a practical standpoint, computational modelling can require long computer runtime, which can be dramatically reduced with mathematical analysis, making complex systems practical to investigate.

REFERENCES

- ARAUJO, R. P. & MCELWAIN, D. L. S. (2004) New insights into vascular collapse and growth dynamics in solid tumors. *J. Theor. Biol.*, **228**, 335–346.
- BARTHA, K. & RIEGER, H. (2006) Vascular network remodeling via vessel cooption, regression and growth in tumors. *J. Theor. Biol.*, **241**, 903–918.
- BUUS, C. L., POURAGEAUD, F., FAZZI, G., JANSSEN, G., MULVANY, M. J. & DE MEY, J. G. (2001) Smooth muscle cell changes during flow-related remodeling of rat mesenteric resistance arteries. *Circ. Res.*, **89**, 180–186.
- CHAPLAIN, M. A. J., MCDUGALL, S. R. & ANDERSON, A. R. A. (2006) Mathematical modeling of tumor-induced angiogenesis. *Annu. Rev. Biomed. Eng.*, **8**, 233–257.
- CHROBAK, K. M., POTTER, D. R. & TIEN, J. (2006) Formation of perfused, functional microvascular tubes in vitro. *Microvasc. Res.*, **71**, 185–196.
- DOR, Y., PORAT, R. M. & KESHET, E. (2001) Vascular endothelial growth factor and vascular adjustments to perturbations in oxygen homeostasis. *Am. J. Physiol. Cell Physiol.*, **280**, C1367–C1374.

- DUMONT, O., LOUFRANI, L. & HENRION, D. (2007) Key role of the no-pathway and matrix metalloprotease-9 in high blood flow-induced remodeling of rat resistance arteries. *Arterioscler. Thromb. Vasc. Biol.*, **27**, 317–324.
- LEHOUX, S. & TEDGUI, A. (1998) Signal transduction of mechanical stresses in the vascular wall. *Hypertension*, **32**, 338–345.
- MCDUGALL, S. R., ANDERSON, A. R. A., CHAPLAIN, M. A. J. & SHERRATT, J. A. (2002) Mathematical modelling of flow through vascular networks: implications for tumour-induced angiogenesis and chemotherapy strategies. *Bull. Math. Biol.*, **64**, 673–702.
- OWEN, M. R., ALARCÓN, T., MAINI, P. K. & BYRNE, H. M. (2009) Angiogenesis and vascular remodelling in normal and cancerous tissues. *J. Math. Biol.*, **58**, 689–721.
- PERKTOLD, K. & RAPPITSCH, G. (1995) Computer simulation of local blood flow and vessel mechanics in a compliant carotid artery bifurcation mode. *J. Biomech.*, **28**, 845–856.
- POZRIKIDIS, C. (2003) *Modeling and Simulation of Capsules and Biological Cells*. Boca Raton, FL: CRC Press.
- PRIES, A. R., REGLIN, B. & SECOMB, T. W. (2001a) Structural adaptation of microvascular networks: functional roles of adaptive responses. *Am. J. Physiol.*, **281**, H1015–H1025.
- PRIES, A. R., REGLIN, B. & SECOMB, T. W. (2005) Remodeling of blood vessels: responses of diameter and wall thickness to hemodynamic and metabolic stimuli. *Hypertension*, **46**, 725–731.
- PRIES, A. R., SECOMB, T. W. & GAEHTGENS, P. (1998) Structural adaptation and stability of microvascular networks: theory and simulation. *Am. J. Physiol.*, **275**, H349–H360.
- PRIES, A. R., SECOMB, T. W. & REGLIN, B. (2001b) Structural adaptation of vascular networks: role of the pressure response. *Hypertension*, **38**, 1476–1579.
- STEPHANOU, A., MCDUGALL, S. R., ANDERSON, A. R. A. & CHAPLAIN, M. A. J. (2006) Mathematical modelling of the influence of blood rheological properties upon adaptative tumour-induced angiogenesis. *Math. Comput. Model.*, **44**, 96–123.
- STROGATZ, S. (2001) *Nonlinear Dynamics and Chaos: With Applications to Physics, Biology, Chemistry and Engineering*. Boulder, CO: Westview Press.